# Structure of $^{130}$La at low and medium spins

M. Ionescu-Bujor,[1] A. Iordăchescu,[1] N. Mărginean,[1] R. Lica,[1] D. Bucurescu,[1] F. Brandolini,[2] D. Deleanu,[1] D. Filipescu,[1] I. Gheorghe,[1] D. Ghiţă,[1] T. Glodariu,[1] R. Mărginean,[1] N. H. Medina,[3] C. Mihai,[1] A. Negret,[1] L. Stroe,[1] and C. A. Ur[1,2]

[1]*Horia Hulubei National Institute of Physics and Nuclear Engineering, Bucharest, Romania*

[2]*Dipartimento di Fisica e Astronomia dell' Universitá and INFN, Sezione di Padova, Padova, Italy*

[3]*Instituto de Física, Universidade de São Paulo, São Paulo, Brazil*

(Received 27 May 2014; revised manuscript received 25 June 2014; published 30 July 2014)

Low- and medium-spin states of the odd-odd nucleus $^{130}$La were studied by in-beam and pulsed-beam $\gamma$-ray spectroscopy using the $^{121}$Sb($^{12}$C,3$n$) and $^{116}$Sn($^{16}$O,$pn$) fusion-evaporation reactions. The decay out of the $\pi h_{11/2} \otimes \nu h_{11/2}$ and $\pi h_{11/2} \otimes \nu g_{7/2}$ rotational structures to the ground state has been elucidated. Spin and parity values have been assigned to most of the newly observed states, as well as to the bandheads of the rotational bands. Two isomeric states were identified and placed in the level scheme, with the characteristics $J^\pi = 5^+$, $E_x = 214.0$ keV, $T_{1/2} = 0.76(9)$ $\mu$s and $J^\pi = 6^+$, $E_x = 319.1$ keV, $T_{1/2} = 33(1)$ ns. The magnetic and quadrupole interactions of the $6^+$ isomeric state have been investigated by the time-differential perturbed $\gamma$-ray angular distribution method. The $g$ factor value, $g(6^+) = +0.48(3)$, and the quadrupole coupling constant in polycrystalline metallic Sn lattice, $\nu_Q(6^+) = 37(4)$ MHz, have been derived. The experimental data are compared with the predictions of two-quasiparticles plus rotor model calculations.

DOI: 10.1103/PhysRevC.90.014323 PACS number(s): 21.10.Ky, 23.20.Lv, 23.35.+g, 27.60.+j

## I. INTRODUCTION

The odd-odd lanthanum isotopes with mass number around 130 belong to a region of transitional nuclei characterized by a variety of interesting phenomena. The nuclei in this mass region are $\gamma$-soft and their shapes are strongly influenced by the quasiparticles in the high-$j$ orbitals. The bands built on the low-$\Omega$ $h_{11/2}$ proton and the high-$\Omega$ $h_{11/2}$ neutron orbitals having different shape-driving effects are of particular interest. One of the most striking features was the observation of the nearly degenerate doublet bands built on the $\pi h_{11/2} \otimes \nu h_{11/2}$ configuration, interpreted as the manifestation of chiral symmetry breaking [1]. This phenomenon has been rather intensively investigated in recent years both experimentally [2–8] and theoretically [9–14].

Another interesting feature of neutron-deficient odd-odd nuclei with $A \approx 130$ is the occurrence of signature inversion at low spins of the $\pi h_{11/2} \otimes \nu h_{11/2}$ bands. The cause of signature inversion has been the subject of investigation in the framework of the particle-triaxial-rotor model [15,16] or the triaxial projected shell model approach [17]. To decide whether signature inversion exists or not, it is important to know the exact spin values of the states in the band. Such information, however, is often unavailable due to the well known difficulties encountered in the studies of odd-odd nuclei, resulting from the occurrence of isomeric decays or the existence of low-energy $\gamma$-ray transitions which are often below observation sensitivity thresholds for typical experiments.

The low-spin states of the odd-odd $^{130}$La nucleus have been investigated in (EC + $\beta^+$) decay of $^{130}$Ce [18]. Spin-parity $3^{(+)}$ has been adopted in Ref. [19] for the ground state, based on the study of $^{130}$Ce $\rightarrow$ $^{130}$La $\rightarrow$ $^{130}$Ba decay [20]. The high spin level scheme of $^{130}$La has been previously investigated in fusion-evaporation reactions and includes two collective bands with a quadrupole deformation $\beta_2 \approx 0.2$, described by the $\pi h_{11/2} \otimes \nu h_{11/2}$ and $\pi h_{11/2} \otimes \nu g_{7/2}$ configurations [21–23], a highly deformed band with $\beta_2 \approx 0.4$ [24], as well as a side band of the $\pi h_{11/2} \otimes \nu h_{11/2}$ yrast band interpreted as resulting from chiral symmetry breaking [25]. Several $\gamma$ rays were assigned to the decay out of the $\pi h_{11/2} \otimes \nu h_{11/2}$ and $\pi h_{11/2} \otimes \nu g_{7/2}$ bands [21,22]. No link, however, was established between the high-spin structures, populated in fusion-evaporation reactions, and the low-spin states, identified following the decay of $^{130}$Ce. Spin-parity $(6^+)$ was tentatively assigned in Ref. [22] to the bandhead of the band described by the $\pi h_{11/2} \otimes \nu h_{11/2}$ configuration. A spin value three units larger was proposed in Ref. [26], on the basis of excitation energy systematics of the yrast band in the doubly-odd $^{124–134}$La by taking as reference the $^{128}$La nucleus, where the spin of the lowest observed state of the band was firmly assigned through experimental spectroscopy [27].

In order to elucidate the structure of the low- and medium-spin states in $^{130}$La, we have studied this nucleus in two heavy-ion fusion-evaporation reaction experiments. As a result of our study, a level scheme was established in which the previously known rotational bands are linked to the ground state. Moreover two low-lying isomeric states were identified and included in the level scheme. After the completion of our experimental studies, Ref. [28] reported the identification in $^{130}$La of an isomer with half-life of 0.74(3) $\mu$s, with unknown excitation energy and spin. This is one of the two isomers observed and investigated in the present work. The experimental details are described in Sec. II, the experimental results are given in Sec. III, while in Sec. IV a theoretical interpretation of the excited states in $^{130}$La, within the two-quasiparticles plus rotor model, is presented.

## II. EXPERIMENTAL DETAILS

The study of the $^{130}$La nucleus was carried out based on data obtained from two independent experiments. In order to construct the decay scheme a $\gamma$-$\gamma$ coincidence experiment was performed using the $^{121}$Sb($^{12}$C,3$n$) reaction at a bombarding

 

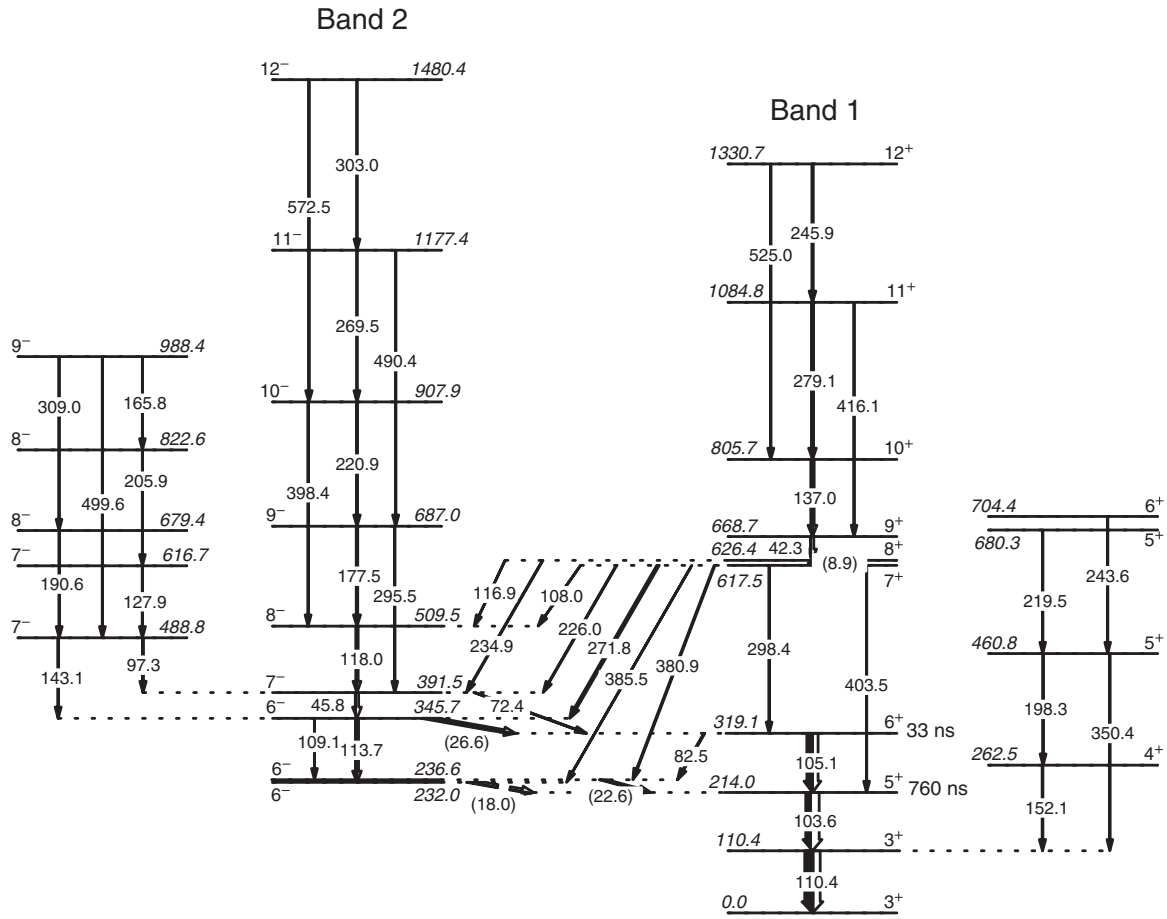


FIG. 1. Partial level scheme of $^{130}$La from the present work. Arrow widths are proportional to transition intensities, while unfilled regions show the extent of internal conversion. The arrows with energy labels in parentheses indicate unobserved tentative transitions.

energy of 50 MeV. The beam was provided by the FN Tandem accelerator of the Horia Hulubei National Institute of Physics and Nuclear Engineering (IFIN-HH) in Bucharest. The target was a 93 mg/cm$^2$ thick metallic Sb foil of natural enrichment placed on a Pb frame. An array consisting of four high-purity germanium (HPGe) planar detectors and five coaxial HPGe detectors of 50% relative efficiency was used for $\gamma$-ray detection. The detectors were placed in three rings at the angles of 143°, 90°, and 45° with respect to the beam axis. The threefold coincidence data were collected in list mode. Single spectra from the planar detectors at 90° and 143° were also taken during the experiment. Energy and efficiency calibrations were performed with standard sources of $^{241}$Am, $^{133}$Ba, and $^{152}$Eu.

Pulsed beam experiments were performed at the XTU Tandem of the Laboratori Nazionali di Legnaro with the aim to investigate the static moments of short-lived isomeric states in neutron deficient nuclei with $A \approx 130$ by applying the time-differential perturbed angular distribution (TDPAD) method. The $^{130}$La nuclei were populated in the $^{116}$Sn($^{16}$O,$pn$) reaction, using a 70 MeV $^{16}$O pulsed beam (pulse width of 3 ns at a repetition period of 800 ns) on isotopically enriched metallic $^{116}$Sn targets. For the $g$-factor determination the target consisted of 0.6 mg/cm$^2$ metallic tin evaporated on a thick Pb backing. The cubic structure of the Pb crystalline lattice allowed the preservation of the nuclear alignment of the recoiled excited $^{130}$La nuclei. The target was placed between the pole tips of an electromagnet. A magnetic field of 32.0(8) kG was applied perpendicular to the beam-detection plane and its direction was periodically reversed in order to reduce the systematic errors. The $\gamma$ rays were detected with two HPGe planar detectors positioned at angles $\pm$135° with respect to the beam direction. In the quadrupole interaction study the target was a $^{116}$Sn thick metallic foil, in which both the beam and the excited La nuclei were stopped. The quadrupole interaction frequency of the isomeric state was obtained from the characteristic spin-dependent pattern of the angular distribution perturbed due to the interaction with the electric field gradient (EFG) of the polycrystalline Sn lattice. Two HPGe planar detectors positioned at the angles of 0° and 90° with respect to the beam direction were used for $\gamma$-ray detection. The time-energy events were list-mode stored separately for each detector.

## III. DATA ANALYSIS AND RESULTS

### A. Level scheme

The construction of the level scheme was based on the analysis of prompt and prompt-delayed $\gamma$-$\gamma$ coincidences.

The coincidence data were sorted offline into various cubes and matrices. A symmetric $E_\gamma$-$E_\gamma$ matrix using all detectors was created with a rather large coincidence gate, around 30 ns, to allow the observation of delayed transitions from short-lived isomers. In order to investigate the low-energy transitions an asymmetric $E_\gamma^{\text{planar}}$-$E_\gamma^{\text{total}}$ matrix was sorted, with the planar detectors incremented on the first axis and all the detectors on the second axis. An $E_\gamma$-$E_\gamma$-$t$ cube was created using the planar detectors. From this cube prompt-delayed and delayed-prompt coincidence matrices were sorted with a time gate of 250 ns put before and after the prompt coincidence peak, respectively. Energy-time matrices gated by $\gamma$ rays of interest were also sorted to study their time behavior for selected feeding transitions.

Information about the transition multipolarities was obtained on the basis of the angular distribution ratio defined as $R_{\text{ADO}} = I_\gamma(143^\circ)/I_\gamma(90^\circ)$. The $\gamma$ intensities, corrected for efficiencies, were derived from the single spectra taken by the planar detectors at 143° and 90°. In the cases of transitions that appeared contaminated in single spectra the analysis was performed using the coincidence data. For this purpose two asymmetric matrices were created, with the detectors at 143° or 90° on the first axis, and all detectors on the second axis. The $\gamma$ intensities were obtained from spectra gated on the axis with all the detectors. In the present experimental conditions, $R_{\text{ADO}}$ values around 0.8 and 1.35 are expected for pure stretched dipole transitions ($\Delta J = 1$) and for stretched quadrupole transitions ($\Delta J = 2$), respectively. The $R_{\text{ADO}}$ values for $\Delta J = 0$ dipole transitions are similar to the ones for the stretched quadrupole transitions.

The level scheme of $^{130}$La derived in the present work is shown in Fig. 1 and its characteristics are given in Table I. The figure includes the lowest-lying states belonging to the positive- and negative-parity rotational structures that were observed in previous works [21,22], labeled as band 1 and band 2, respectively. These bands are linked to the ground state through a rather complex scheme containing several low-energy transitions, some of them not observed, as well as two isomeric states. In addition the level scheme includes states of medium spin not connected with the rotational bands, that were observed for the first time.

The $\gamma$-ray intensities were derived from the spectrum obtained by summing the two single spectra taken by the planar detectors at 90° and 143°, as well as from the symmetric $E_\gamma$-$E_\gamma$ matrix. The single spectrum was essential for determining the intensities of isomeric transitions, that could not be derived from the coincidence spectra. We derived $R_{\text{ADO}}$ values for almost all observed transitions. For several low-energy transitions, the multipolarity determination was carried out by deriving the internal-conversion coefficients using the intensity balance relation $I_\gamma^1(1+\alpha_T^1) = I_\gamma^2(1+\alpha_T^2)$, with $I_\gamma^{1,2}$ the $\gamma$-ray intensity and $\alpha_T^{1,2}$ the total conversion coefficient of the cascade transitions labeled with indices 1 and 2.

Illustrative spectra obtained by gating on selected transitions in the total symmetric $\gamma$-$\gamma$ matrix are presented in Fig. 2. In these spectra peaks were observed at 33.2(2) and 37.7(2) keV, identified as the La $K_\alpha$ and $K_\beta$ x-ray lines due

TABLE I. Characteristics of the level scheme of $^{130}$La displayed in Fig. 1: excitation energies of levels $E_i$, $\gamma$-ray energies $E_\gamma$, spins and parities of the initial and final levels $J_i^\pi$ and $J_f^\pi$, relative intensities $I_\gamma$, and angular distribution ratios $R_{\text{ADO}}$ of the $\gamma$ rays. The experimental errors of the relative intensities for the strong transitions are of the order of 5%, while for weak lines the errors can rise up to 50%.

| $E_i$ (keV) | $E_\gamma$ (keV) | $J_i^\pi$ | $J_f^\pi$ | $I_\gamma$ | $R_{\text{ADO}}$ |
|---|---|---|---|---|---|
| 110.4 | 110.4(2) | $3^+$ | $3^+$ | 100.0 | 1.20(15) |
| 214.0 | 103.6(2)[a] | $5^+$ | $3^+$ | 57.4 | 0.99(3)[a] |
| 232.0 | 18.0(2)[b] | $6^-$ | $5^+$ | 6.9[b] | |
| 236.6 | 22.6(2)[b] | $6^-$ | $5^+$ | 6.8[b] | |
| 262.5 | 152.1(2) | $4^+$ | $3^+$ | 6.1 | 0.87(10) |
| 319.1 | 105.1(2)[a] | $6^+$ | $5^+$ | 68.2 | 1.02(3)[a] |
| | 82.5(2)[a] | | $6^-$ | 7.5 | 0.97(6)[a] |
| 345.7 | 113.7(2) | $6^-$ | $6^-$ | 21.2 | 1.36(7) |
| | 109.1(2) | | $6^-$ | 1.3 | |
| | 26.6(2)[b] | | $6^+$ | 15.0[b] | |
| 391.5 | 72.4(2) | $7^-$ | $6^+$ | 5.0 | 0.72(9) |
| | 45.8(2) | | $6^-$ | 3.4 | |
| 460.8 | 198.3(2) | $5^+$ | $4^+$ | 3.4 | 0.92(12) |
| | 350.4(3) | | $3^+$ | 1.2 | |
| 488.8 | 97.3(2) | $7^-$ | $7^-$ | 3.9 | 1.21(13) |
| | 143.1(2) | | $6^-$ | 3.5 | 0.84(7) |
| 509.5 | 118.0(2) | $8^-$ | $7^-$ | 16.5 | 0.75(5) |
| 616.7 | 127.9(2) | $7^-$ | $7^-$ | 3.1 | 1.53(20) |
| 617.5 | 108.0(2) | $7^+$ | $8^-$ | 1.8 | 0.81(16) |
| | 226.0(2) | | $7^-$ | 6.6 | 1.41(11) |
| | 271.8(2) | | $6^-$ | 25.2 | 0.85(5) |
| | 298.4(2) | | $6^+$ | 2.9 | 0.81(15) |
| | 380.9(2) | | $6^-$ | 9.5 | 0.78(9) |
| | 385.5(2) | | $6^-$ | 0.6 | |
| | 403.5(2) | | $5^+$ | 3.3 | 1.37(13) |
| 626.4 | 8.9(2)[b] | $8^+$ | $7^+$ | 0.2[b] | |
| | 116.9(2) | | $8^-$ | 0.2 | |
| | 234.9(2) | | $7^-$ | 6.2 | 0.79(6) |
| 668.7 | 42.3(2) | $9^+$ | $8^+$ | 2.7 | |
| 679.4 | 190.6(2) | $8^-$ | $7^-$ | 3.6 | 0.85(12) |
| 680.3 | 219.5(2) | $5^+$ | $5^+$ | 1.0 | 1.25(15) |
| 687.0 | 177.5(2) | $9^-$ | $8^-$ | 14.4 | 0.87(7) |
| | 295.5(2) | | $7^-$ | 3.2 | 1.20(15) |
| 704.4 | 243.6(2) | $6^+$ | $5^+$ | 1.1 | 0.80(12) |
| 805.7 | 137.0(2) | $10^+$ | $9^+$ | 27.4 | 0.73(7) |
| 822.6 | 205.9(2) | $8^-$ | $7^-$ | 1.5 | 0.70(18) |
| 907.9 | 220.9(2) | $10^-$ | $9^-$ | 9.6 | 0.66(6) |
| | 398.4(2) | | $8^-$ | 3.8 | 1.55(30) |
| 988.4 | 165.8(2) | $9^-$ | $8^-$ | 1.1 | |
| | 309.0(2) | | $8^-$ | 1.3 | 0.55(17) |
| | 499.6(2) | | $7^-$ | 3.4 | 1.46(29) |
| 1084.8 | 279.1(2) | $11^+$ | $10^+$ | 23.2 | 0.82(6) |
| | 416.1(2) | | $9^+$ | 2.1 | 1.29(19) |
| 1177.4 | 269.5(2) | $11^-$ | $10^-$ | 4.6 | 0.62(8) |
| | 490.4(2) | | $9^-$ | 6.5 | 1.33(8) |
| 1330.7 | 245.9(2) | $12^+$ | $11^+$ | 12.7 | 0.82(4) |
| | 525.0(3) | | $10^+$ | 5.8 | 1.36(8) |
| 1480.4 | 303.0(2) | $12^-$ | $11^-$ | 3.8 | 0.75(9) |
| | 572.5(2) | | $10^-$ | 10.2 | 1.45(15) |

[a]Isomeric transition with an isotropic angular distribution.
[b]$\gamma$-ray energy and intensity inferred from the level scheme.

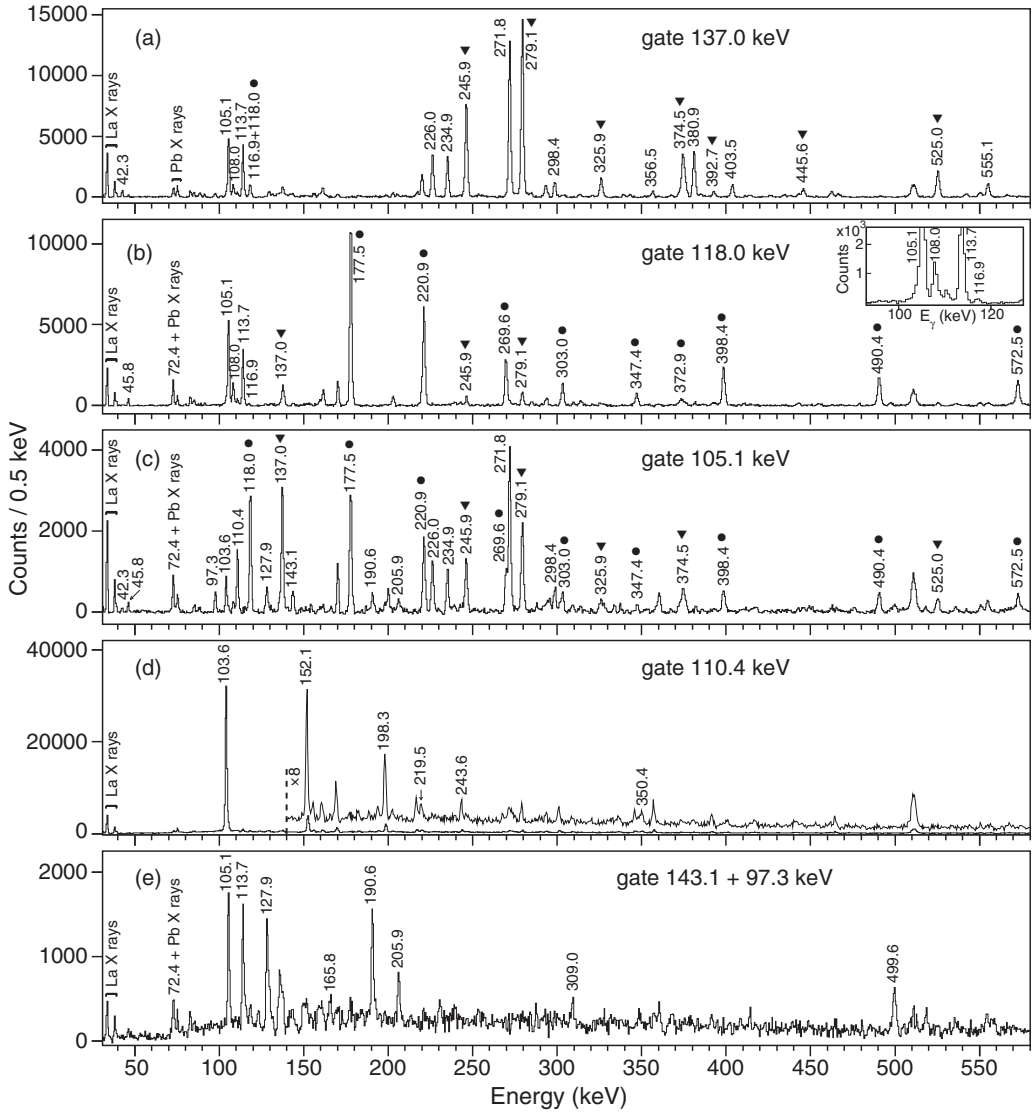


FIG. 2. Coincidence spectra from the symmetric $E_\gamma$-$E_\gamma$ matrix. The $\gamma$ rays in $^{130}$La are labeled by the energy. Peaks marked with full triangles and full circles belong to bands 1 and 2, respectively. The inset evidences the presence of the weak 116.9 keV transition in coincidence with the 118.0 keV $\gamma$ ray.

to internal conversion. Spectra shown in panels (a) and (b)—obtained by gating on the $\gamma$ lines of 137 and 118 keV, the lowest lying transitions in the bands 1 and 2, respectively—display the $\gamma$ rays belonging to the bands, as well as the $\gamma$ rays of their decay out. The in-band transitions are marked with full triangles and full circles in the figure. In the present experiment we observed ten states belonging to band 1 and eight states belonging to band 2.

The $\gamma$ lines of 105, 108, 114, 226, 235, 271, and 380 keV found in the decay-out of band 1 [21,22], as well as the $\gamma$ lines of 298 and 403 keV, not seen in [22], but reported in [21], are evidenced in the spectrum gated by the 137-keV $\gamma$ ray. The 46 and 72-keV low-energy transitions seen in Ref. [22] in coincidence with transitions belonging to band 2 are observed in the spectrum gated by the 118-keV line. Note that in our experiment the peak of 72.4 keV is superimposed on the 72.8-keV Pb $K_{\alpha 2}$ x-ray line appearing as contaminant due to ionization of the Pb frame.

A new low-energy transition of 42.3 keV was identified in coincidence with the transitions of band 1, as seen in Fig. 2(a). The 42.3-keV $\gamma$ ray was also found in coincidence with all transitions assigned in the decay-out of the band. Illustrative spectra registered by the planar detectors obtained from the asymmetric $E_\gamma^{\text{planar}}$-$E_\gamma^{\text{total}}$ matrix, are shown in Fig. 3. Based on these coincidence relationships, the new transition of 42.3 keV was placed at the bottom of band 1.

Isomeric transitions were investigated in delayed spectra produced from the prompt-delayed matrix by gating on various $\gamma$ rays of the $^{130}$La level scheme. Delayed $\gamma$ rays of 103.6 and 110.4 keV were found in coincidence with the 113.7-keV $\gamma$ line, as seen in Fig. 4(a). When gating on the other $\gamma$ lines belonging to the bands or to their decay out, delayed transitions

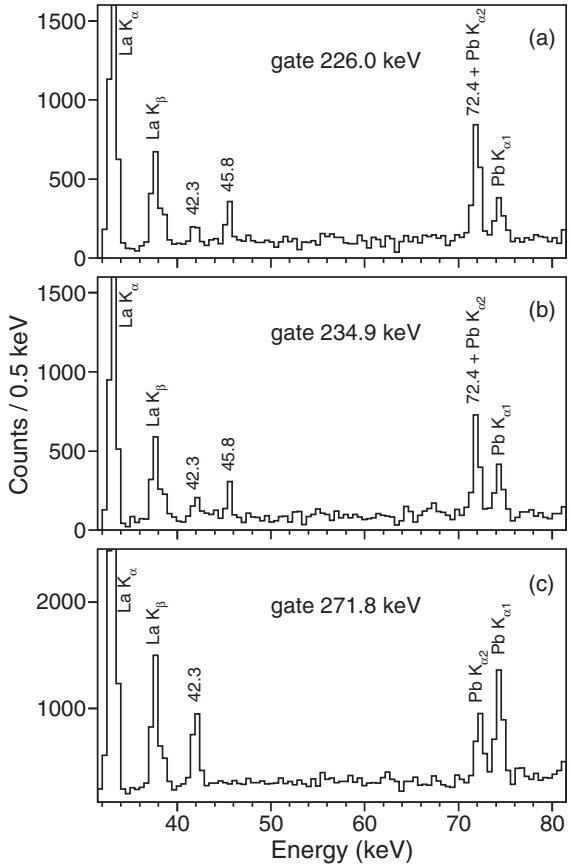


FIG. 3. Spectra registered by the planar detectors, obtained from the $E_\gamma^{\text{planar}}$-$E_\gamma^{\text{total}}$ matrix, showing the coincidence relations between selected transitions in the decay-out of band 1 and the low-energy transitions of 42.3, 45.8, and 72.4 keV.

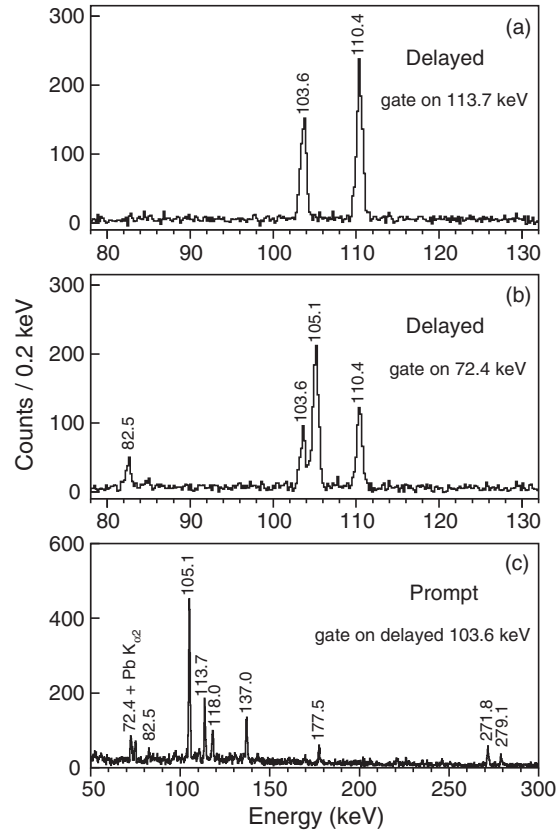


FIG. 4. Spectra registered by the planar detectors showing prompt-delayed $\gamma$-$\gamma$ coincidences in $^{130}$La. (a) Delayed $\gamma$ rays in coincidence with the prompt 113.7-keV transition. (b) Delayed $\gamma$ rays in coincidence with the prompt 72.4-keV transition. (c) Prompt $\gamma$ rays in coincidence with the delayed 103.6 keV transition.

of 82.5 and 105.1 keV were also observed [Fig. 4(b)]. The time spectra of the 82.5 and 105.1-keV $\gamma$ rays exhibit the same half-life of 33(3) ns, as illustrated in Fig. 5. On the other hand, the time spectra of the 103.6- and 110.4-keV $\gamma$ rays, obtained by gating on a sum of feeding transitions, indicated a much longer isomer lifetime, of the order of hundreds of ns. A precise lifetime determination was not possible in the $\gamma$-$\gamma$ coincidence experiment. The half-life of this longer-lived isomer has been measured as $T_{1/2} = 0.76(9)$ $\mu$s in the pulsed beam measurements (see next subsection). It agrees with the half-life 0.74(3) $\mu$s reported recently for the 104 and 110 keV decays [28].

The ground-state spin and parity of $^{130}$La have been adopted as $3^{(+)}$ [19]. The spin value assignment is based on the feeding by electron capture of $2^+$ and $4^+$ states in $^{130}$Ba [20,29]. Many low-spin states have been populated in $^{130}$La following the decay of $^{130}$Ce [18]. The first excited state was found at 110.4 keV, with a half-life of 17(5) ns and $J^\pi = (1^+,2,3^+)$ [18,19]. The second excited state, placed at an excitation energy of 131.1 keV, was reported to be an isomer with a half-life of 77(10) ns [18]. This state has spin-parity $1^+$ and decays to the ground state by a $\Delta J = 2$ transition. By using the measured half-life and the total conversion coefficients taken from Ref. [30], we estimated the reduced

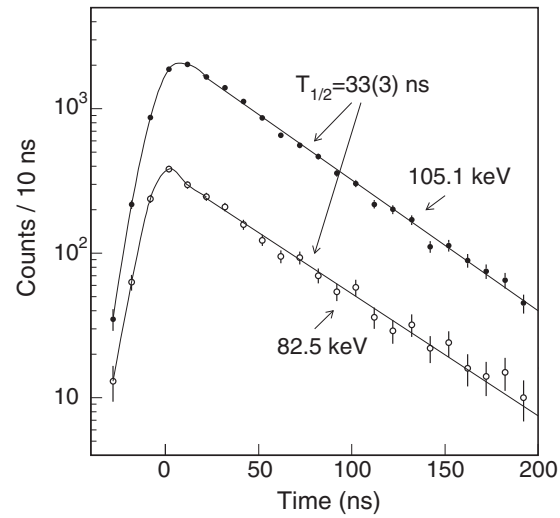


FIG. 5. Time spectra of the 105.1- and 82.5-keV $\gamma$ rays de-exciting the state at excitation energy of 319.1 keV, obtained by gating on the sum of 72, 118, and 137 keV transitions.

TABLE II. Experimental intensity ratios $I_\gamma^{103.6}/I_\gamma^{110.4}$ and $I_\gamma^{152.1}/I_\gamma^{110.4}$ compared with calculated ratios for various multipolarities, using theoretical conversion coefficients taken from Ref. [30].

| 110.4 keV | $E1$ | $M1$ | $E2$ | Experiment |
|---|---|---|---|---|
| 103.6 keV | | | | |
| $E1$ | 0.97 | 1.50 | 1.98 | 0.68(5) |
| $M1$ | 0.60 | 0.92 | 1.21 | |
| $E2$ | 0.43 | 0.66 | 0.87 | |
| 152.1 keV | | | | |
| $E1$ | 1.10 | 1.69 | 2.23 | 1.49(15) |
| $M1$ | 0.88 | 1.36 | 1.80 | |

transition probabilities $B(E2)(131.1\ \text{keV}) = 2.8(4)$ W.u. and $B(M2)(131.1\ \text{keV}) = 82(12)$ W.u. The $M2$ multipolarity has to be ruled out as the corresponding transition strength is much higher than the upper limit of 1 W.u. recommended for this mass region [31]. An $E2$ character is therefore established for the 131.1-keV transition de-exciting the $1^+$ isomeric state, which gives strong support for the positive-parity assignment to the $^{130}$La ground state.

The 110.4-keV $\gamma$ ray is the most intense observed transition in our experiment and was identified as the transition from the first excited level in $^{130}$La to the ground state [19]. Note that this is the only transition reported in the (EC + $\beta^+$) decay of $^{130}$Ce that was observed in the present study. The 110.4-keV $\gamma$ ray is coincident with the 103.6-keV $\gamma$ ray, as well as with the new transitions of 152.1, 198.3, 219.5, 243.6, and 350.4 keV, as shown in Fig. 2(d). The 103.6-keV isomeric transition was placed above the 110.4-keV level, establishing the energy of the 0.76 $\mu$s isomeric state at an excitation energy of 214.0 keV. The other newly observed transitions have been included in the structure shown in the right side of the level scheme of Fig. 1 (see below).

The $R_{\text{ADO}}$ ratio of the 103.6 keV isomeric transition, derived from single spectra, was found to be $\approx$1, indicating an isotropic angular distribution due to the perturbation of the nuclear alignment by the strong interaction with the EFG of the polycrystalline lattice of the antimony target during the isomer lifetime. An isotropic behavior has been also found in single spectra for the 110.4-keV transition, as it has a dominant component from the isomer feeding. The $R_{\text{ADO}}$ ratio could be determined for this transition from coincidence spectra obtained by using the sum of gates on the 152.1- and 198.3-keV transitions. The obtained $R_{\text{ADO}}$ value (see Table I) indicated either a stretched quadrupole transition $1^+ \rightarrow 3^+$(g.s.) or a $\Delta J = 0$ $3^+ \rightarrow 3^+$(g.s.) dipole transition. The multipolarities of the 103.6- and 110.4-keV transitions have been studied by comparing the experimental ratio $I_\gamma^{103.6}/I_\gamma^{110.4}$ of $\gamma$ intensities derived from delayed spectra with calculated values using theoretical conversion coefficients. As seen in Table II, agreement between the experimental and calculated intensity ratios is obtained for two sets of multipolarities $\sigma(110.4\ \text{keV})/\sigma(103.6\ \text{keV})$, namely $M1/E2$ and $E1/M1$. Additional information was obtained from the intensities of the 110.4- and 152.1-keV $\gamma$ rays, derived by gating on the 198.4-keV line. From the comparison of the experimental intensity ratio $I_\gamma^{152.1}/I_\gamma^{110.4}$ with calculated values an $E1$ character for the 110.4 keV is ruled out (see Table II). Therefore the multipolarities $M1$-110.4 keV and $E2$-103.6 keV have been assigned, leading to spin-parity $3^+$ and $5^+$ for the states at 110.4 and 214.0 keV, respectively. We note that the time spectrum of the 110.4-keV $\gamma$ rays gated by the 103.6-keV transition showed only a prompt component, corresponding to a half-life shorter than 10 ns. The half-life of 17(5) ns reported previously for the 110.4-keV state in (EC + $\beta^+$) decay of $^{130}$Ce [18] is not confirmed in our work.

As shown in Fig. 4(c), the delayed 103.6-keV transition is coincident with the 82.5 and 105.1-keV $\gamma$ lines. The 33 ns isomer was therefore placed at an excitation energy of 319.1 keV, feeding the 0.76 $\mu$s isomer through the 105.1-keV transition, and a new state at 236.6 keV through a 82.5 keV transition. An unobserved transition of 22.6 keV from the 236.6 keV to the 214.0 keV was tentatively included in the level scheme, supported by the observed coincidence between the 82.5- and 103.6-keV transitions. As in the case of 103.6-keV transition, no information could be obtained on the multipolarity of the 105.1- and 82.5-keV transitions from $R_{\text{ADO}}$ values, due to the loss of nuclear alignment produced in quadrupole interaction. $J^\pi = 6^+$ has been assigned to the 319.1-keV isomeric state based on results of TDPAD studies that are presented in the next subsection. Thus the spin value is based on the dipole character of the 105.1-keV transition for which a negative $A_2$ angular distribution coefficient has been measured in the quadrupole interaction study, while the positive parity is supported by the analysis of the $g$ factor determined for this state.

An excited state at 617.5 keV was established on the basis of the observed 298.4-keV $\gamma$ ray coincident with the 105.1-keV transition [Fig. 2(c)]. This state is linked to the $5^+$ isomer via the 403.5-keV transition assigned as $E2$ on the basis of its $R_{\text{ADO}}$ value. Therefore we assign a spin-parity $7^+$ for the 617.5-keV state. The dipole character of the 298.4-keV transition to the $6^+$ isomer supports this assignment. The 617.5 keV level is also de-excited by the 108.0-, 226.0-, 271.8-, 380.9-, and 385.5-keV transitions, feeding five states at excitation energy of 509.5, 391.5, 345.7, 236.6, and 232.0 keV, respectively. The 391.5- and 509.5-keV states, connected by the 118.0 keV transition, are the bandhead and the first excited state of band 2, respectively. The total conversion coefficient of the 108.0-keV transition was derived from the relative $\gamma$-ray intensities of the 108.0–118.0 keV cascade transitions in a spectrum gated by the 137.0-keV transition, by assuming an $M1$ character for the 118.0-keV transition. The experimental value is compared in Table III with the theoretical conversion coefficients for $E1$ and $M1$ multipolarity, and leads to an $E1$ assignment to the 108.0-keV transition from the $7^+$ level. The negative parity of the states of band 2 is therefore clearly established.

The 391.5-keV bandhead is deexcited by the low-energy transition of 45.8 keV to the 345.7-keV state that is also populated by the 271.8 keV transition from the yrast $7^+$ state. The bandhead is connected to the $6^+$ isomer at 319.1 keV through a $\gamma$ transition of 72.4 keV. An $M1$ character of the 45.8-keV transition was assigned on the basis of its conversion coefficient, deduced from the intensity balance at

TABLE III. Conversion coefficients of four low-energy transitions. The theoretical $\alpha_{\rm tot}^{E1}$ and $\alpha_{\rm tot}^{M1}$ values were taken from Ref. [30]. The $\alpha_{\rm tot}^{\rm exp}$ values are derived by taking the 137.0- and 118.0-keV transitions as $M1$ and the 72.4-keV transition as $E1$.

| $E_\gamma$ (keV) | $\alpha_{\rm tot}^{E1}$ | $\alpha_{\rm tot}^{M1}$ | $\alpha_{\rm tot}^{\rm exp}$ |
|---|---|---|---|
| 42.1 | 2.39 | 13.0 | 14.3(29) |
| 45.8 | 1.95 | 10.3 | 11.8(24) |
| 97.3 | 0.25 | 1.17 | 1.34(35) |
| 108.0 | 0.19 | 0.87 | 0.17(5) |

the 391.5-keV level in a spectrum gated by the 177.5-keV $\gamma$ ray (see Table III).

The $R_{\rm ADO}$ values determined for the 271.8- and 226.0-keV transitions allowed us to assign spin-parities $6^-$ and $7^-$ to the 345.7- and 391.5-keV states, respectively. The 345.7-keV level is deexcited by the 109.1- and 113.7-keV transitions to the states at 236.6 and 232.0 keV fed also by the 380.9- and 385.5-keV transitions, respectively. In view on the observed coincidence between the 45.8- and 105.1-keV transitions [Fig. 2(c)], a 26.6-keV unobserved transition from the 345.7-keV state to the $6^+$ isomeric state is included, On the basis of the stretched dipole character of the 380.9-keV transition from the $7^+$ yrast state, spin 6 was assigned to the state at 236.6-keV excitation energy. The state is also populated by the 82.5-keV transition from the $6^+$ isomer. The $R_{\rm ADO}$ value of the 113.7-keV transition feeding the 232.0-keV states is consistent with either a stretched electric quadrupole transition or a $\Delta J = 0$ transition, which allows a spin assignment of 4 or 6 for this level. Based on the absence of transitions to the $3^+$ ground and 110.4-keV states, we assign a spin value of 6. The assignment is also supported by the fact that a spin 4 for the 232.0-keV state would imply $\Delta J = 3$ for the 385.5-keV transition that is excluded by lifetime considerations. A negative parity was tentatively assigned to the 236.6- and 232-keV states, as they have a population pattern similar to that of the higher-lying negative-parity states. Moreover we note that a positive-parity assignment would imply that the $6^+$ isomeric state is not yrast positive parity, in disagreement with its high population yield. The 236.6- and 232-keV states are deexcited by unobserved transitions of 22.6- and 18.0-keV transitions to the $5^+$ isomeric state.

The transition of 234.9 keV has the same coincidence relationships as the 226.0-keV transition [see Figs. 2(b), 2(c), 3(a), and 3(b)] and was placed such as to feed the $7^-$ head of band 2, from a level at 626.4 keV. Based on the stretched dipole character of the 234.9-keV transition, a spin 8 is assigned to this new level. It is also deexcited by the weak transition of 116.9-keV coincident with the 118.0-keV transition [shown in the inset of Fig. 2(a)]. To explain the observed coincidence relationships between the in-band transitions and transitions decaying the 617.5-keV state, an unobserved 8.9-keV transition from the 626.4-keV state to this level is tentatively included.

The newly observed 42.3-keV transition is placed above the 626.4-keV state, thus defining the energy of the bandhead of band 1 at 668.7 keV. The multipolarity of the 42.3-keV transition was assigned as $M1$ on the basis of its conversion coefficient, deduced from the intensity balance at the bandhead level in a spectrum gated by the 279.1-keV $\gamma$ ray, assuming an $M1$ character for the 137.0 keV transition (see Table III). Thus we assign spin-parity $9^+$ to the head of band 1.

A new structure of negative parity levels was established in $^{130}$La involving the transitions of 97.3, 127.9, 143.1, 190.6, 205.9, 165.8, 309.0, and 499.8 keV (see the left side of the level scheme of Fig. 1). It is built on a state at 488.8 keV linked to the $7^-$ 391.5-keV bandhead of band 2 and to the $6^-$ 345.7-keV state by the 97.3- and 143.1-keV transitions, respectively. The $R_{\rm ADO}$ values of these transitions support spin 7 for the 488.8-keV state. An $M1$ character was established for the 97.3-keV transition based on the conversion coefficient deduced from intensity balance at the 391.5-keV level, in a spectrum gated by the 127.9-keV $\gamma$ ray (Table III). We thus assign $J^\pi = 7^-$ to the 488.8-keV state. Spins in the new structure are based on $R_{\rm ADO}$ values for the involved transitions. The highest spin is $9^-$ at 966.4 keV, deexcited by the 499.6-keV electric quadrupole transition. The five new transitions coincident with the 110.4-keV $\gamma$ ray [Fig. 2(d)] were included in the positive parity structure, shown in the right side of the level scheme of Fig. 1. The state at 460.8 keV was assigned spin-parity $5^+$ as it deexcites via the $E2$ 350.4-keV transition to the first excited $3^+$ state. This state is fed by the 219.5- and 243.6-keV dipole transitions with $R_{\rm ADO}$ values consistent with $\Delta J = 0$ and $\Delta J = 1$, respectively, pointing to spins $5^+$ and $6^+$ for the states at 680.3 and 704.4 keV excitation energies.

### B. *g* factor and quadrupole interaction strength of the $6^+$ isomeric state

In offline analysis of data registered in the pulsed beam measurements, two-dimensional matrices of energy versus time were formed for each detector. From these matrices delayed energy spectra have been created to investigate the isomeric transitions. Illustrative delayed $\gamma$ spectra obtained in the quadrupole interaction measurement for two successive time intervals of 350 ns after the $^{16}$O beam pulse are shown in Fig. 6. They reveal the presence of the 82.5-, 105.1- and 103.6-keV isomeric transitions of $^{130}$La. The 110.4-keV $\gamma$ ray from the first excited state in $^{130}$La has a strong long-lived component coming from the (EC + $\beta^+$) decay of $^{130}$Ce. In the experiment the short-lived isomeric states $9/2^-$, $T_{1/2} =$ 60 ns and $7^-$, $T_{1/2} = 92$ ns in $^{129,130}$Ce nuclei have also been populated. The static moments determined for these isomers were reported previously [32,33].

The decay curves for the 105.1- and 103.6-keV $\gamma$ rays obtained by summing the time spectra registered at 0° and 90° are shown in Fig. 7 together with the least-squares fits. The half-life of 33(1) ns determined for the 105.1-keV $\gamma$ ray is in excellent agreement with the value derived from $\gamma$-$\gamma$ coincidences for the $6^+$ isomeric state. The 103.6-keV $\gamma$ ray exhibits a growth-decay curve that includes the population from the upper $6^+$ isomer. A half-life of 0.76(9) $\mu$s was derived for the $5^+$ isomeric state.

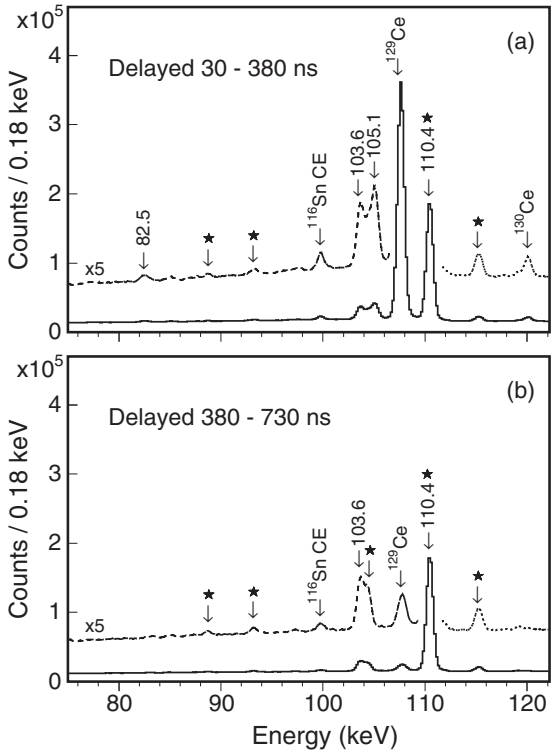


FIG. 6. Delayed $\gamma$ spectra corresponding to two successive time intervals after the $^{16}$O beam pulse, obtained using the thick tin target. The delayed transitions in $^{130}$La are marked by energies. Transitions deexciting other short lived isomers are indicated by the corresponding nuclei. The $\gamma$ lines coming from long-lived activities are marked with a star.

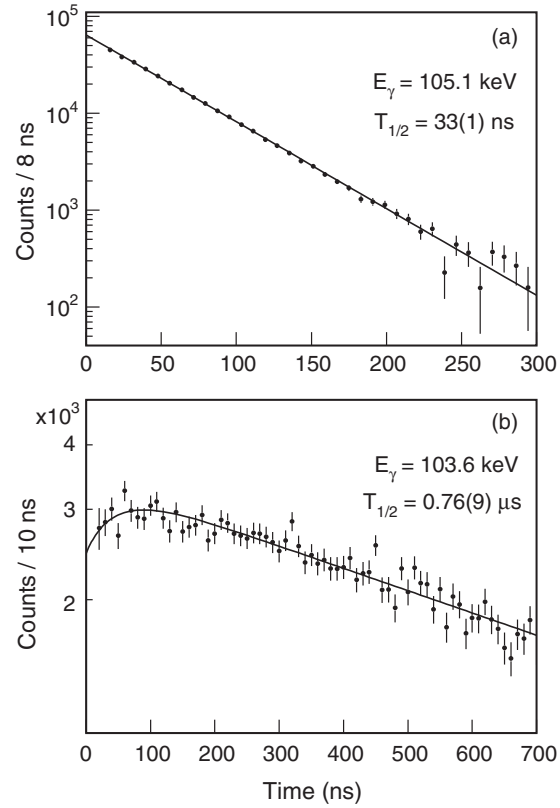


FIG. 7. Experimental time spectra for the 105.1- and 103.6-keV $\gamma$ rays and least-squares fits.

In the magnetic interaction (MI) measurement the time spectra corresponding to the 105.1-keV $\gamma$ ray obtained for each of the two magnetic-field orientations were used to form the experimental modulation ratio

$$R^{MI}_{\rm exp}(t) = \frac{N^{\uparrow}(t) - N_{\downarrow}(t)}{N^{\uparrow}(t) + N_{\downarrow}(t)}, \tag{1}$$

which was least-squares fitted to the expression

$$R^{MI}_{\rm theo}(t) = \tfrac{3}{4} A_2 \cos 2(\phi - \omega_L t) \tag{2}$$

with the angular distribution coefficient $A_2$, the Larmor frequency $\omega_L = gH\mu_n/\hbar$, and the phase $\phi$ depending on the detector position angle and the beam bending in the magnetic field as free parameters. The experimental modulation ratio obtained in an external magnetic field of 32.0(8) kG is shown in Fig. 8 together with the calculated one. The $g$ factor which results from the derived Larmor frequency is $g(6^+) = +0.48(3)$. The sign of the $g$ factor was determined from the direction of the rotation of the angular distribution pattern, considering a negative angular distribution coefficient $A_2$ as derived from the quadrupole interaction measurement (see below). The diamagnetic and Knight shift corrections were not applied, as they are small (about 1%), similar in magnitude, and opposite in sign.

The quadrupole interaction (QI) frequency of the isomeric state was obtained from the characteristic spin-dependent pattern of the angular distribution perturbed due to the interaction with the electric field gradient of the polycrystalline Sn lattice. The time spectra of the 105.1-keV $\gamma$ ray, background subtracted and normalized, were used to construct the experimental ratio

$$R^{QI}_{\rm exp}(t) = \frac{N(t,0^\circ) - N(t,90^\circ)}{N(t,0^\circ) + N(t,90^\circ)}, \tag{3}$$

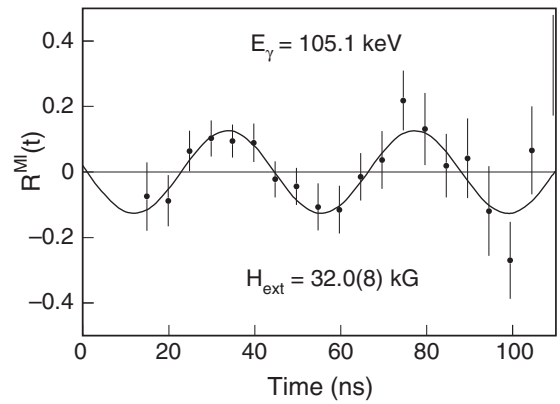


FIG. 8. Experimental modulation ratio for the 105.1-keV $\gamma$ ray deexciting the $6^+$ isomer in $^{130}$La in external magnetic field and the least-squares fit.

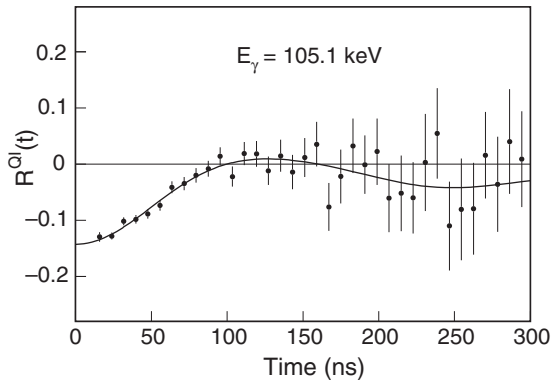


FIG. 9. Experimental TDPAD spectrum showing the quadrupole interaction of the $6^+$ isomer in polycrystalline metallic Sn lattice and least-squares fit.

which was least-squares fitted to the expression

$$R^{QI}_{\text{theo}}(t) = \frac{3}{4} A_2 \sum s_{2n} \cos(n\omega_0 t) \tag{4}$$

with the angular distribution coefficient $A_2$ and the frequency $\omega_0$ as free parameters. The spin-dependent $s_{2n}$ coefficients in the theoretical expression (4) were calculated according to the formulas in Ref. [34] for an axially symmetric randomly oriented EFG. The quadrupole frequency decreases quadratically with the spin $J$ and, for an integer spin, is given by $\omega_0 = 3\pi\nu_Q/2J(2J-1)$, where $\nu_Q = QV_{zz}/h$ is the quadrupole coupling constant depending on the quadrupole moment $Q$ and the EFG strength $V_{zz}$.

The experimental ratio is shown in Fig. 9 together with the corresponding fitted curve. Due to the short lifetime of the isomer, it was not possible to evidence the full quadrupole period $T_0 = 2\pi/\omega_0$ and only the structure at the beginning of the modulation pattern could be observed. The angular distribution coefficient has been determined as $A_2 = -0.19(2)$, indicating a dipole multipolarity for the 105.1-keV transition. The frequency $\omega_0$ resulting from the least-squares fit led to the value $\nu_Q(6^+) = 37(4)$ MHz for the quadrupole coupling constant of the $6^+$ isomeric state in $^{130}$La implanted in polycrystalline metallic Sn lattice at room temperature.

In order to derive the electric quadrupole moment from the measured quadrupole coupling constant $\nu_Q$ one needs to know the strength $V_{zz}$ of the electric field gradient experienced by the excited nuclei. The EFG strength of a metallic lattice at the site of dilute impurities depends on both the host and the impurity nuclei [35]. At present, however, the calibration of the electric field gradient for La nuclei in the polycrystalline tin lattice is not known, preventing us from deducing the value of the electric quadrupole moment.

Experimental ratios were constructed also for the 103.6-keV $\gamma$ ray deexciting the $5^+$ isomer, however no modulation effect could be observed in both the magnetic and the quadrupole interaction studies. This was most probably due to the fact that in this case the pulsed beam repetition period was comparable to the isomer half-life, and therefore an incoherent superposition of modulation patterns coming from successive beam pulses occurred, leading to the smearing out of the modulation amplitude.

## IV. DISCUSSION

The properties of low- and moderate-spin states in $^{130}$La are dominated by the interplay between collective and single particle motion. According to the observed intrinsic configurations in neighboring odd-$A$ nuclei, the active single-particle states are the $[550]1/2^-$, $[420]1/2^+$, and $[422]3/2^+$ proton states, as well as the $[514]9/2^-$, $[411]1/2^+$, $[400]1/2^+$, and $[404]7/2^+$ neutron states. Indeed, the lowest-energy bands in $^{129}$La are assigned as based on rotation-aligned $[550]1/2^-$ Nilsson state of $h_{11/2}$ parentage, as well as on the $[420]1/2^+$ and $[422]3/2^+$ states of $d_{5/2}$ and $g_{7/2}$ parentage [36]. Similarly, the lowest-energy bands in $^{129}$Ba are assigned to the deformation-aligned $[514]9/2^-$ state derived from the $h_{11/2}$ subshell, to the $[411]1/2^+$ and $[400]1/2^+$ orbitals from the $s_{1/2}$ and $d_{3/2}$ states, and to the $[404]7/2^+$ state of $g_{7/2}$ parentage [37].

In order to understand the structure of the observed states in the odd-odd-$^{130}$La nucleus, we have performed calculations using the two-quasiparticles plus rotor model (TQRM) [38], in which the two quasiparticles are treated explicitly in addition to the collective even-even core. The used single-particle potential was of the modified oscillator type with the $\kappa$ and $\mu$ parameters taken from Ref. [39]. The pairing gap and the Fermi levels were derived from a BCS treatment of pairing. The interaction strengths were obtained by multiplying 0.95 to the standard strengths [40] in order to take into account the blocking effect. The calculations were performed by considering a prolate axial-symmetric shape of the core. We adopted the deformation parameters $\epsilon_2 = 0.20$ and $\epsilon_4 = 0.02$, predicted for $^{130}$La ground state in the macroscopic-microscopic calculations tabulated in Ref. [41]. The core moments of inertia were calculated in such a way that the experimental energy of 284 keV of the $2^+$ state of the even-even $^{128}$Ba nucleus was reproduced. In evaluating the magnetic moments, an effective $g_s$ factor of $0.7g_s^{\text{free}}$ has been used and $g_R$ has been taken as $Z/A$. Quadrupole moments of the core were calculated macroscopically. Another model parameter, the coefficient $\xi$ representing the attenuation of the Coriolis matrix elements, has been varied between 1 (no attenuation) and 0.6. Calculations were carried out either without an effective residual proton-neutron ($p$-$n$) interaction, or by using a zero-range interaction of the form

$$V_{pn} = 15.75b^3\delta(\mathbf{r_p} - \mathbf{r_n})(u_0 + u_1\sigma_\mathbf{p}\sigma_\mathbf{n}), \tag{5}$$

where $b$ is the oscillator length $b = 1.006 \times A^{1/6}$ fm and $\sigma$ is the Pauli spin matrix. The interaction strength parameters $u_0 = -7.2$ MeV and $u_1 = -0.8$ MeV proposed in [42] for this region of nuclei have been used in the calculations. We note that the same residual interaction was used by Tajima in his analysis of signature inversion of $A \approx 130$ odd-odd nuclei [15].

The low-lying positive-parity states have been calculated assuming that both the valence proton and neutron are located in the deformed $gds$ orbitals of the $N = 4$ shell. Positive-parity states have been also calculated with the odd particles in

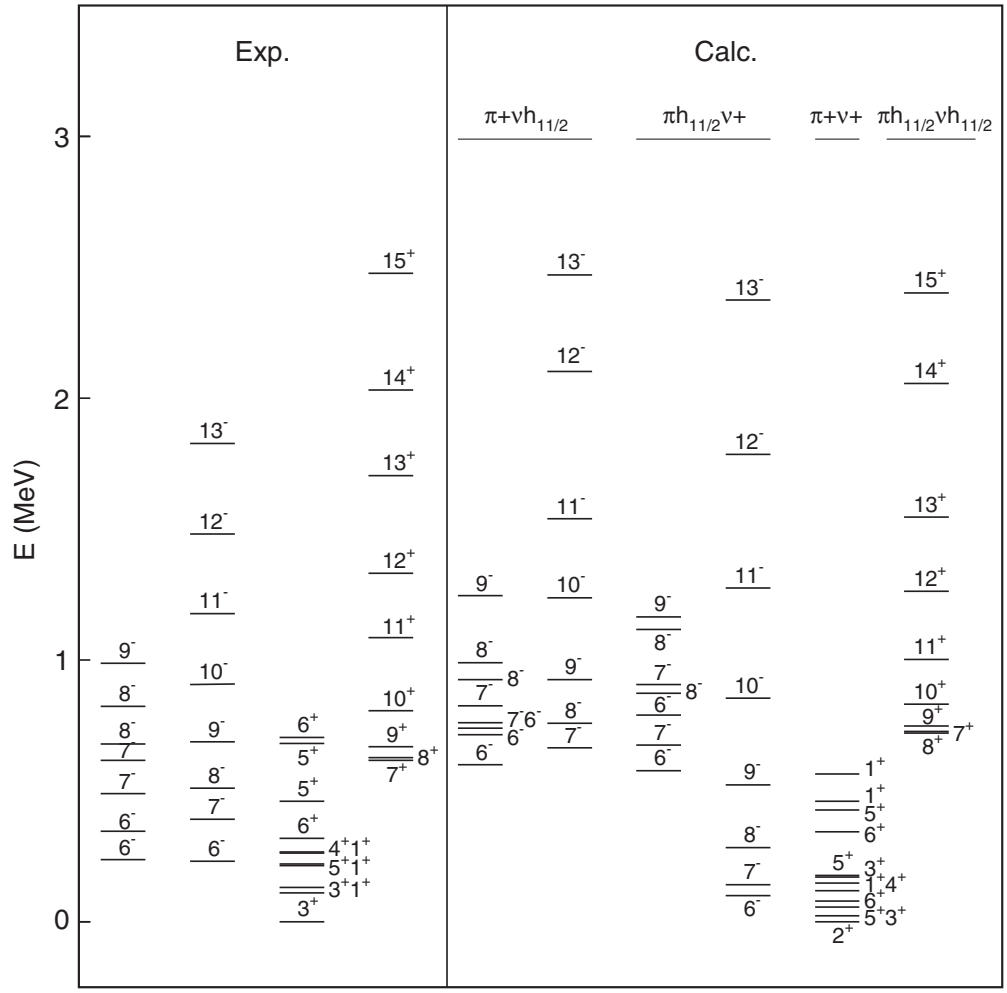


FIG. 10. Experimental partial level scheme of $^{130}$La (from Ref. [19] and present work) compared to two-quasiparticles plus rotor model calculations performed at deformation parameters $\epsilon_2 = 0.20$ and $\epsilon_4 = 0.02$. The valence proton and neutron configurations used in the calculations are shown in the figure. The proton and neutron located in the positive-parity orbitals of the $N = 4$ shell are denoted with $\pi+$ and $\nu+$, respectively. Calculations were performed for $\xi = 1$ and without $p$-$n$ residual interaction.

the states of the $h_{11/2}$ subshell. In order to describe the negative-parity states it was assumed that the odd proton occupies orbitals in the $1h_{11/2}$ subshell and the odd neutron is in the $N = 4$ shell orbitals. Calculations were also performed with the valence proton located in the $gds$ shell and the valence neutron in the $1h_{11/2}$ subshell.

The experimental excitation energies of low- and medium-spin states in $^{130}$La are compared in Fig. 10 with the energies calculated with the two-quasiparticles plus rotor model, for $\xi = 1$ and without a $p$-$n$ residual interaction. Besides the states observed in the present study, we have included in the analysis the lowest-lying $J^\pi = 1^+$ states observed in (EC + $\beta^+$) decay of $^{130}$Ce [18,19]. As seen in the figure, the relative positions of the structures involving different proton-neutron couplings are satisfactorily accounted for by the calculations. In particular the low- and medium-spin positive-parity states described by the valence proton and neutron in the deformed $gds$ orbitals are calculated to be lowest in energy, in accordance with the experimental findings.

In the present work the spins of the band described by the $\pi h_{11/2} \otimes \nu h_{11/2}$ coupling have been firmly established. With these assignments the experimental even-spin levels of the band are favored energetically, rather than the odd-spin members that are expected to be favored in the case of normal signature splitting. Therefore, the spin values assigned in this work prove the existence of signature inversion in $^{130}$La and give further support to the spin assignments made for the $\pi h_{11/2} \otimes \nu h_{11/2}$ bands in the odd-odd La isotopes on the basis of excitation energy systematics [26]. As illustrated in Fig. 10, the TQRM satisfactorily calculates the excitation energy of the bandhead, however a normal signature splitting is predicted, with the odd-spin levels lowered in energy. To reproduce the observed signature inversion, we performed calculations in which a zero-range $p$-$n$ interaction was included. The results are shown in Fig. 11. It is seen that the inclusion of the residual $p$-$n$ interaction produces a lowering of the even-spin level energies, in accordance with the experimental findings. The experimental energies are well reproduced by

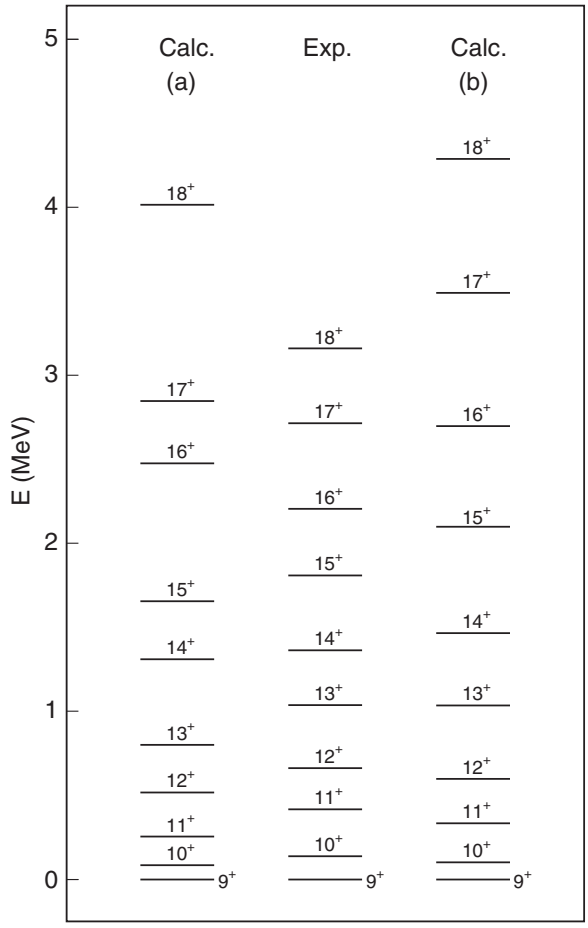


FIG. 11. Experimental yrast positive-parity band of $^{130}$La (from Ref. [19] and present work) compared to two-quasiparticles plus rotor model calculations performed without (a) and with (b) *p-n* residual interaction. The excitation energies are relative to that of the $9^+$ bandhead. Calculations were performed for $\xi = 1$.

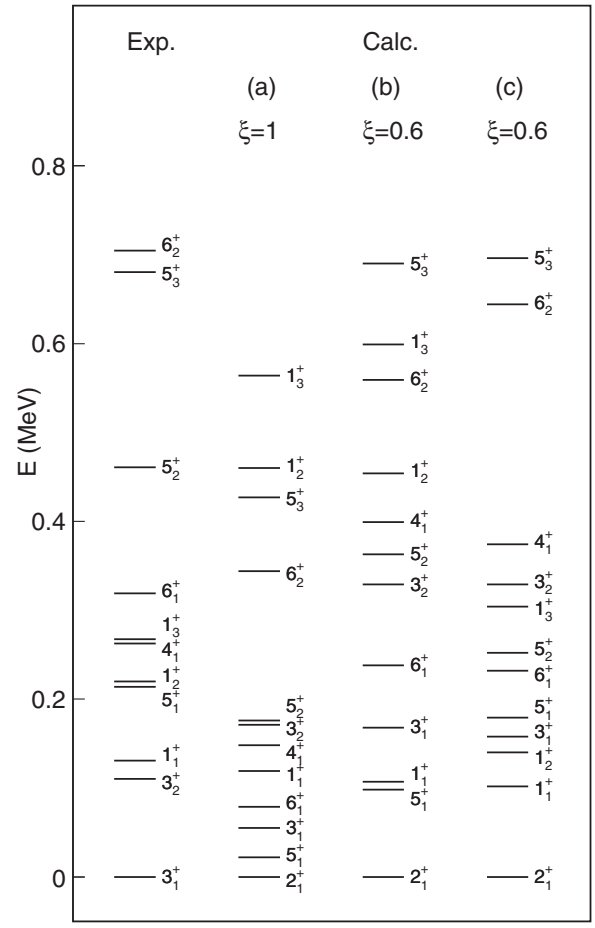


FIG. 12. Experimental low-lying positive-parity states of $^{130}$La (from Ref. [19] and present work) compared to two-quasiparticles plus rotor model calculations performed without [(a) and (b)] and with (c) *p-n* residual interaction. The values of the attenuation of the Coriolis matrix elements $\xi$ used in the calculations are shown in the figure.

the calculations at lower spins, however at high spins the calculations overpredict the energies of the levels.

The negative-parity states observed in $^{130}$La were described within TQRM by coupling the odd proton in low-Ω orbitals from the $h_{11/2}$ subshell with the odd neutron in the positive-parity orbitals. The neutron $[404]7/2^+$ orbital was found to dominate the structure of the yrast negative-parity band, while the wave functions of non-yrast states involve the $[413]5/2^+$ and $[402]3/2^+$ neutron orbitals. As illustrated in Fig. 10, the states produced by coupling the proton in the positive-parity orbitals with the neutron in the $h_{11/2}$ state are predicted at higher energies. Moreover there is a pronounced signature splitting in the calculated band, in disagreement with the experimental data.

The TQRM calculations indicated that the structure of the low-lying positive-parity states is dominated by the neutron $[404]7/2^+$ orbital, coupled with proton deformed orbitals from the $d_{5/2}$ and $g_{7/2}$ spherical states. As seen in Fig. 10 the calculated excited levels appear depressed in energy compared with the observed states, excepting the $1_2^+$ and $1_3^+$ states that are predicted at higher energy. Moreover the sequence of level spins is not in agreement with the experimental data. We performed also calculations by applying an attenuation of the Coriolis interaction and by including the *p-n* residual interaction. The results are illustrated in Fig. 12. The energies calculated with a Coriolis attenuation factor $\xi = 0.6$ are higher compared with those calculated for $\xi = 1$, however the sequence of spins is almost unchanged. With the inclusion of the *p-n* zero-range residual interaction the description of several states is improved. Thus the $1_2^+$ and $1_3^+$ states are pushed down in energy, while the $5_1^+$ state is calculated above the $3_1^+$ state, in accordance with the experimental findings. On the other hand the energies of the $2_1^+$, $3_1^+$, $3_2^+$, and $6_1^+$ states are not modified when the residual interaction is included. In all calculations a spin-parity $2^+$ is predicted for the ground-state, while the adopted spin-parity is $3^+$. No state with $J^\pi = 2^+$ has been observed experimentally. This could indicate that the $2^+$ states are located above the 110.4 keV $3^+$ state and therefore could not be fed in the decay of the high-spin states lying above.

The observed discrepancies between the experimental and calculated excitation energies appear to indicate that the used zero-range $p$-$n$ residual interaction is not fully adequate. The effective residual $p$-$n$ interaction in odd-odd deformed rare earth nuclei was studied in Ref. [43], and improvements were found when a finite-range central force combined with spin-polarized and long-range components were included in the effective $p$-$n$ force. The matrix elements of these interactions are usually fitted to experimental data on excited nuclear levels and are state dependent. It would be very interesting to perform TQRM calculations for $^{130}$La by using this complex effective residual $p$-$n$ interaction. At present, however, no information on matrix elements of this interaction exist in the $A \approx 130$ region.

The analysis of the wave functions indicates that the first $5^+$ state arises from the coupling of the $[411]3/2^+$ proton orbital with the $[404]7/2^+$ neutron orbital, while the structure of the first $6^+$ state has a dominant $K = 6, \pi[413]5/2^+ \otimes \nu[404]7/2^+$ configuration, with small contributions from the $K = 5$, $\pi[422]3/2^+ \otimes \nu[404]7/2^+$ and $\pi[411]3/2^+ \otimes \nu[404]7/2^+$ couplings. These configurations are assigned to the observed $5^+$ and $6^+$ isomeric states. The $g$ factors calculated for these states are $g_{\rm calc}(5^+) = +0.74$ and $g_{\rm calc}(6^+) = +0.47$. The experimental $g$ factor of the $6^+$ isomer, $g_{\rm exp}(6^+) = +0.48(3)$, is very well reproduced by the TQRM calculations. It is worthwhile to mention that the calculated $g$ factors for the $6^-$ states, $g_{\rm calc}(6^-) = +0.99$ and $+0.19$ for configurations involving positive neutron orbitals and positive proton orbitals, respectively, differ considerably from the experimental value. This gives support to the positive-parity assignment for the isomeric state.

With the presently adopted deformation parameters of Ref. [41], the TQRM calculations predict for the two isomeric states spectroscopic quadrupole moment values of $Q_{\rm calc}(5^+) = 2.0$ $e$b and $Q_{\rm calc}(6^+) = 2.1$ $e$b. By using the calculated quadrupole moment and the quadrupole coupling constant $\nu_Q(6^+) = 37(4)$ MHz determined in the present work for the $6^+$ isomer, we estimate the strength of the electric field gradient for La impurity in tin lattice at room temperature as $V_{zz}(\mathrm{LaSn}) = 0.73(8) \times 10^{21}$ V/m$^2$. We note, however, that in view of the strong dependence of the calculated quadrupole moment value on the deformation, for a reliable EFG calibration an independent determination of the deformation through lifetime measurements in the rotational bands of $^{130}$La would be necessary.

By using the half-lives and $\gamma$ branchings determined in the present work and the total conversion coefficients taken from Ref. [30], we estimated the reduced transition probabilities for the isomeric transitions:

$$B(M1)(105.1\ \mathrm{keV}) = 2.66(13) \times 10^{-4}\ \mathrm{W.u.},$$
$$B(E1)(82.5\ \mathrm{keV}) = 1.02(11) \times 10^{-6}\ \mathrm{W.u.},$$
$$B(E2)(103.6\ \mathrm{keV}) = 0.58(7)\ \mathrm{W.u.}$$

These values are consistent with the transitions strengths reported in nuclei of this mass region [31]. The TQRM predicts a reduced transition probability $B(M1)(6^+ \rightarrow 5^+) = 6 \times 10^{-4}$ W.u., in remarkable agreement with the experimental value. Recently a 53-keV $(8^-) \rightarrow (8^+)$, 486 ns $E1$ transition has been identified in $^{132}$Pr, that corresponds to a reduced transition probability of $1.48 \times 10^{-6}$ W.u. [28]. This is very close to the $B(E1)(6^+ \rightarrow 6^-)$ value obtained in the present work.

## V. SUMMARY

The excited states of $^{130}$La were populated via the $^{121}$Sb($^{12}$C,3$n$) and $^{116}$Sn($^{16}$O,$pn$) fusion-evaporation reactions. The main aim of the present study was to find links between the high-spin rotational bands and the low-spin states populated in $\beta$ decay. Moreover, the study focused on the investigation of the short-lived isomeric decays. We have analyzed the $\gamma$-ray prompt and delayed coincidences and the angular distribution ratios. Furthermore, the internal conversion coefficients of several low-energy transitions have been derived from intensity balances. As a result of the present work, the decay out of the $\pi h_{11/2} \otimes \nu h_{11/2}$ and $\pi h_{11/2} \otimes \nu g_{7/2}$ bandheads to the ground state has been elucidated and unambiguous spin and parity values have been assigned to most levels. In addition new medium-spin positive- and negative-parity states not connected with the known rotational bands have been identified. The spin values assigned in this work to the $\pi h_{11/2} \otimes \nu h_{11/2}$ band members prove the existence of signature inversion in $^{130}$La. Two low-lying isomeric states have been included in the level scheme and their properties have been investigated in detail. A half-life $T_{1/2} = 0.76(9)$ $\mu$s has been determined for the level at 214.0 keV assigned as $J^\pi = 5^+$. A second isomeric state, with a half-life $T_{1/2} = 33(1)$ ns, was placed at $E_x = 319.1$ keV and assigned as $J^\pi = 6^+$. The pulsed beam TDPAD method has been applied to determine the $g$ factor and the quadrupole interaction strength of the $6^+$ isomer implanted in the polycrystalline metallic Sn lattice at room temperature.

The structure of the observed states in the odd-odd $^{130}$La nucleus is discussed within the two-quasiparticles plus rotor model. The $\pi h_{11/2} \otimes \nu h_{11/2}$ and $\pi h_{11/2} \otimes \nu g_{7/2}$ configurations previously assigned to the yrast and yrare rotational bands are confirmed by the present calculations. The inclusion of an effective proton-neutron residual interaction is found essential to account for the observed signature inversion in the $\pi h_{11/2} \otimes \nu h_{11/2}$ band. The structure of the low-lying positive-parity states is dominated by the neutron $[404]7/2^+$ orbital, coupled with proton deformed orbitals from the $d_{5/2}$ and $g_{7/2}$ spherical states. The $g$ factor of the $6^+$ isomer and the $B(M1)$ reduced transition probability of its deexciting transition are remarkably well reproduced by the two-quasiparticles plus rotor model calculations.

## ACKNOWLEDGMENTS

We would like to thank the staffs of the FN Tandem of IFIN-HH in Bucharest and XTU Tandem of Laboratori Nazionali di Legnaro for the high quality of the delivered beams. We are indebted to Dr. I. Ragnarsson for the two-quasiparticles plus rotor model code. The work was supported by the Romanian Ministry of National Education, Project PN-II-ID-PCE-2011-3-0140.

[1] S. Frauendorf and J. Meng, Nucl. Phys. A **617**, 131 (1997).
[2] C. M. Petrache, D. Bazzacco, S. Lunardi, C. Rossi Alvarez, G. de Angelis, M. De Poli, D. Bucurescu, C. A. Ur, P. B. Semmes, and R. Wyss, Nucl. Phys. A **597**, 106 (1996).
[3] K. Starosta *et al.*, Phys. Rev. Lett. **86**, 971 (2001).
[4] A. J. Simons *et al.*, J. Phys. G: Nucl. Part. Phys. **31**, 541 (2005).
[5] D. Tonev *et al.*, Phys. Rev. Lett. **96**, 052501 (2006).
[6] E. Grodner *et al.*, Phys. Rev. Lett. **97**, 172501 (2006).
[7] J. Timár *et al.*, Phys. Rev. C **84**, 044302 (2011).
[8] I. Kuti *et al.*, Phys. Rev. C **87**, 044323 (2013).
[9] V. I. Dimitrov, S. Frauendorf, and F. Dönau, Phys. Rev. Lett. **84**, 5732 (2000).
[10] K. Higashiyama and N. Yoshinaga, Eur. Phys. J. A **33**, 355 (2007).
[11] D. Almehed, F. Dönau, and S. Frauendorf, Phys. Rev. C **83**, 054308 (2011).
[12] I. Hamamoto, Phys. Rev. C **88**, 024327 (2013).
[13] K. Higashiyama and N. Yoshinaga, Phys. Rev. C **88**, 034315 (2013).
[14] G. H. Bhat, R. N. Ali, J. A. Sheikh, and R. Palit, Nucl. Phys. A **922**, 150 (2014).
[15] N. Tajima, Nucl. Phys. A **572**, 365 (1994).
[16] V. Kumar, S. Kumar, S. Kumar, Z. Hasan, B. S. Koranga, D. Kumar, D. Negi, and L. Angus, Int. J. Mod. Phys. E **20**, 1455 (2011).
[17] Z. C. Gao, Y. S. Chen, and Y. Sun, Phys. Lett. B **634**, 195 (2006).
[18] S. Xu *et al.*, Z. Phys. A **356**, 35 (1996).
[19] B. Singh, Nucl. Data Sheets **93**, 33 (2001).
[20] C. Gerschel, M. Pautral, R. A. Ricci, J. Teillac, and J. Van Horenbeeck, Nuovo Cimento **37**, 1756 (1965).
[21] E. S. Paul, C. W. Beausang, D. B. Fossan, R. Ma, W. F. Piel, Jr., N. Xu, and L. Hildingsson, Phys. Rev. C **36**, 1853 (1987).
[22] M. J. Godfrey, Y. He, I. Jenkins, A. Kirwan, P. J. Nolan, D. J. Thornley, S. M. Mullins, and R. Wadsworth, J. Phys. G: Nucl. Part. Phys. **15**, 487 (1989).
[23] M. J. Godfrey, Y. He, I. Jenkins, A. Kirwan, P. J. Nolan, D. J. Thornley, S. M. Mullins, R. Wadsworth, and R. A. Wyss, J. Phys. G: Nucl. Part. Phys. **15**, 671 (1989).
[24] M. J. Godfrey, Y. He, I. Jenkins, A. Kirwan, P. J. Nolan, R. Wadsworth, and S. M. Mullins, J. Phys. G: Nucl. Part. Phys. **15**, L163 (1989).
[25] T. Koike, K. Starosta, C. J. Chiara, D. B. Fossan, and D. R. LaFosse, Phys. Rev. C **63**, 061304(R) (2001).
[26] Y. Liu, J. Lu, Y. Ma, S. Zhou, and H. Zheng, Phys. Rev. C **54**, 719 (1996).
[27] T. Hayakawa, J. Lu, J. Mukai, T. Saitoh, N. Hasimoto, T. Komatsubara, and K. Furuno, Z. Phys. A **352**, 241 (1995).
[28] M. J. Taylor *et al.*, Phys. Rev. C **86**, 044310 (2012).
[29] C. T. Königshofen, K. Jessen, A. Gade, I. Wiedenhöver, H. Meise, and P. von Brentano, Phys. Rev. C **64**, 037302 (2001).
[30] T. Kibédi, T. W. Burrows, M. B. Trzhaskovskaya, P. M. Davidson, and C. W. Nestor, Jr., Nucl. Instrum. Methods Phys. Res. Sect. A **589**, 202 (2008).
[31] P. M. Endt, At. Data Nucl. Data Tables **26**, 47 (1981).
[32] M. Ionescu-Bujor, A. Iordachescu, F. Brandolini, M. De Poli, N. H. Medina, P. Pavan, M. N. Rao, and C. Rossi Alvarez, Nucl. Phys. A **633**, 459 (1998).
[33] M. Ionescu-Bujor, A. Iordachescu, F. Brandolini, M. De Poli, N. H. Medina, P. Pavan, M. N. Rao, and C. Rossi Alvarez, Phys. Rev. C **60**, 024316 (1999).
[34] E. Dafni, R. Bienstock, M. H. Rafailovich, and G. D. Sprouse, At. Data Nucl. Data Tables **23**, 315 (1979).
[35] R. Vianden, Hyperfine Interact. **35**, 1079 (1987).
[36] Y. He, M. J. Godfrey, I. Jenkins, A. J. Kirwan, S. M. Mullins, P. J. Nollan, E. S. Paul, and R. Wadsworth, J. Phys. G: Nucl. Part. Phys. **18**, 99 (1992).
[37] J. Gizon, A. Gizon, and J. Meyer-ter-vehn, Nucl. Phys. A **277**, 464 (1977).
[38] I. Ragnarsson and P. B. Semmes, Hyperfine Interact. **43**, 425 (1988).
[39] J. Y. Zhang, N. Xu, D. B. Fossan, Y. Liang, R. Ma, and E. S. Paul, Phys. Rev. C **39**, 714 (1989).
[40] S. G. Nilsson, C. F. Tsang, A. Sobiczewski, Z. Szymański, S. Wycech, C. Gustafsson, I.-L. Lamm, P. Möller, and B. Nilsson, Nucl. Phys. A **131**, 1 (1969).
[41] P. Möller, J. R. Nix, W. D. Myers, and W. J. Swiatecki, At. Data Nucl. Data Tables **59**, 185 (1995).
[42] P. B. Semmes and I. Ragnarsson, in *Proceedings of the International Conference on High Spin Physics and Gamma-soft Nuclei, Pittsburgh, 1990*, edited by J. X. Saladin, R. A. Sorensen, and C. M. Vincent (World Scientific, Singapore, 1991), p. 500.
[43] J. P. Boisson, R. Piepenbring, and W. Ogle, Phys. Rep. **26**, 99 (1976).